Journal of Nuclear Materials 547 (2021) 152806

Contents lists available at ScienceDirect

Journal of Nuclear Materials

journal homepage: www.elsevier.com/locate/jnucmat

High temperature Cr-Zr interaction of two types of Cr-coated Zr alloys in inert gas environment

Jianqiao Yang[a,b,*], Ulrike Stegmaier[a], Chongchong Tang[a], Martin Steinbrück[a], Mirco Große[a], Shuzhong Wang[b], Hans Jürgen Seifert[a]

[a] Institute for Applied Materials (IAM), Karlsruhe Institute of Technology (KIT), D-76021 Karlsruhe, Germany
[b] Key Laboratory of Thermo-Fluid Science and Engineering of MOE, School of Energy and Power Engineering, Xi'an Jiaotong University, 28 Xianning West Road, Xi'an 710049, PR China

ARTICLE INFO

Article history:
Received 30 September 2020
Revised 13 December 2020
Accepted 10 January 2021
Available online 12 January 2021

Keywords:
Accident tolerant fuel cladding
Magnetron sputtering
Cold spraying
Chromium coating
Zirconium alloy
Kinetic parameters

ABSTRACT

The Cr-Zr interaction of two types of Cr coated Zr alloy accident tolerant fuel (ATF) claddings, deposited by cold spraying and magnetron sputtering, was studied in argon in the temperature range from 1100 to 1300°C. A tube furnace with a sample lock system was used for fast exchanging samples at test temperature. Inter-diffusion between the coating and the substrate results in the formation of an intermetallic $ZrCr_2$ layer and a solid solution layer beneath. Some pores were formed on the interlayer by a Kirkendall-type mechanism. The interlayer growth rate of cold sprayed samples was always slightly higher than that of magnetron sputtered samples in the same condition. Moreover, the temperature-dependent consumption coefficient of the Cr coating was calculated and fitted to an Arrhenius function. The dissolution and precipitation behavior of Cr in the Zr substrate and the diffusion behavior of Zr in Cr coating were also studied.

1. Introduction

After the Fukushima-Daiichi accidents, the interests have been boosted to develop advanced accident tolerant fuel (ATF) cladding materials for improved performance during operation and under accident scenarios. Several approaches are being pursued to improve the oxidation performance of cladding materials in LOCA (Loss of coolant accident) and severe accident (SA) conditions. Chromium coatings are worldwide under consideration as a near-term solution for ATF cladding. The Cr coating on zirconium alloy has exhibited good performance under accident scenarios [1]: excellent high temperature oxidation resistances, relatively low neutron absorption cross section compared with other candidate coating materials, equal thermal expansion coefficient with Zr, high melting point and relatively high eutectic temperature with Zr. This package of positive properties makes Cr coating a promising candidate as a coating for ATF cladding tubes.

Many researches have been done on the growth kinetics of the Cr_2O_3 layer on Cr coated Zr alloy in normal operation conditions [2–4], LOCA conditions [2,5–10] and beyond LOCA conditions [11,12]. As a protective layer, the consumption rate of Cr coating under accident scenarios is a key parameter on how long the coated cladding can survive in extreme high temperature environment. The outer side of the coating is mainly consumed by the oxidation of chromium. Moreover, the inner side of the coating can be consumed by diffusing of chromium into the Zr substrate and forming a Cr-Zr interlayer. This diffusion process, which is driven by high temperature, should not be neglected. In contrast to oxidation tests, there are only few studies focusing on the Cr-Zr interaction. Brachet et al. [2] found that the consumption kinetics of the Cr coating by formation of oxide film and by diffusion into the substrate at 1200°C are nearly identical. Xiang et at. [13] studied the growth kinetics of the Cr-Zr interlayer up to 850°C, and they found that the interlayer growth approximately obeys the parabolic law. However, the experiment by Xiang et al. was done using a Cr-Zr diffusion couple, which is different from the coating situation. Moreover, the annealing temperature is far lower than the typical temperature in LOCA accidents [14]. Yeom et al. [9] conducted a series of oxidation tests on a cold spraying Cr coated Zry-4 alloy in high-temperature steam environment, and they measured the thickness of the Cr-Zr interlayer after exposure. A parabolic law on the growth of the interlayer was also obtained. However, almost all measured values of the interlayer thickness were higher than the estimated value after exposure, which is due to the fact that the drastic oxidation of the uncoated side of the tube specimens released a large amount of heat; therefore, the actual temperature

* Corresponding author.
E-mail address: jianqiao.yang@aliyun.com (J. Yang).

https://doi.org/10.1016/j.jnucmat.2021.152806
0022-3115/

Table 1
The description of the samples.

No.	Shape	Diameter	Radian	Length	Coating method
1	Circular arc	id=8 mm; od=9.1 mm	120°	3 mm	Cold spraying
2	Circular arc	id=8 mm; od=9.1 mm	120°	3 mm	Magnetron sputtering

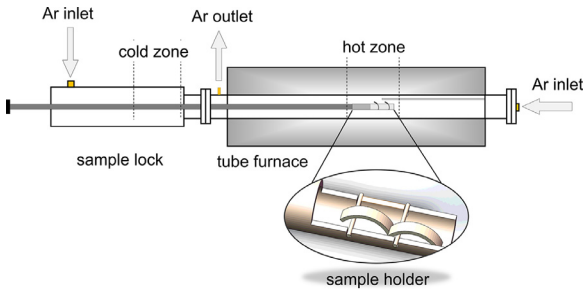

Fig. 1. Schematic diagram of the tube furnace with the sample lock system. The structure of the sample holder is shown as an enlarged figure.

of the specimen was higher than the nominal target temperature during the exposure process.

Magnetron sputtering and cold spraying are widely used for the preparation of Cr coating, which can produce dense and adherent coating with different thicknesses [1,15]. In a cold spraying process, high-velocity micron-sized Cr particles hit on a Zr substrate and adhered to the substrate via severe plastic deformation [16,17]. As for a magnetron sputtering process, Cr atoms are ejected from the target by ion bombardment and deposited onto substrates inside a vacuum chamber [18,19]. The difference of the coating methods leads to different coating qualities, which can affect the interaction between the coating and the substrate in high-temperature environment. However, there is no published literature concerning the effect of coating methods on the interdiffusion behavior between the Cr coating and the Zr substrate.

This paper focuses on the high temperature Cr-Zr interaction of Cr-coated Zry-4 alloys. A cold sprayed (CS) sample and a magnetron sputtered (MS) sample were used. The diffusion tests were done in inert gas environment to eliminate the influence of the oxidation reaction. The growth kinetics of the interlayer was determined, and the temperature-dependent consumption coefficient of the Cr coating was calculated and fitted to an Arrhenius function. Moreover, the dissolution and precipitation behavior of Cr in the Zr substrate was studied at different cooling rates. This study could provide useful data to estimate the life span of the coating in LOCA or even more serious accident scenarios.

2. Materials and methods

A cold sprayed tube sample (coating thickness: around 32 μm) and a magnetron sputtered tube sample (coating thickness: around 13 μm) were used in the diffusion tests [3,20]. The as-received tube samples were cut into slices with a thickness of 3 mm, and then cut into three pieces. Detailed dimension information of the samples are summarized in Table 1. All the cutting works were done by an automatic cut-off machine (ATM Brillant 250) with a diamond cutting wheel. The cutting rate was 0.05 mm/s, and the samples were protected by cooling water during cutting.

The test system contains a gas cylinder, a gas flow controller, a tube furnace, a mass spectrometer, a control center and a computer. Detailed introduction of this system can be found in a previous paper [21]. A sample lock system was used with the tube furnace, allowing exchange of samples at high temperature. The structure of the tube furnace with the sample lock is shown in Fig. 1.

Table 2
Conditions used for the tests.

Temperature	Exposure time (min)
1100°C	10, 30, 60, 120, 150
1150°C	30, 60
1200°C	3, 5, 10, 30, 60, 120, 150
1250°C	20, 30
1300°C	1, 3, 5, 10, 20, 30, 50, 60 120

One CS and one MS sample were placed in the sample lock simultaneously in each experiment. Argon (6N, 20 L/h) was injected into the heating chamber from both the tube furnace and the sample lock. When the oxygen concentration in the argon off-gas was less than 0.05%, the specimens were pushed from the sample lock into the hot zone of the furnace. As soon as the target exposure time was achieved, the samples were pulled off to the cold zone. Then, the samples were kept in the cold zone for several minutes for cooling down in argon environment. Through this system, the Cr-Zr interaction during heating and cooling periods can be avoided, and the annealing time can be precisely controlled. The test matrix is listed in Table 2.

After the tests, the specimens were embedded in epoxy resin. SiC paper was used to reduce half of the length of the specimens to eliminate the edge effect. The cross sections of the specimens were observed by a scanning electron microscopy (SEM, Philips XL30S) and an optical microscopy (OM). The Smileview software [22] was used for measuring the thickness of the Cr-Zr interlayer and the residual Cr coating layer. In each image, ten points were evenly spaced for thickness measurements. The average value of ten measurements was determined as the final thickness of the layer.

3. Results and discussion

3.1. Surface morphology

Fig. 2 shows the typical cross section morphologies of the samples before and after annealing. The figures were observed by SEM in secondary electron (SE) mode. Fig. 2(a) is the cross section morphology of the as received CS sample. The interface of the coating and the substrate is uneven, and the average thickness of the coating is about 32 $\pm$ 3 μm. The annealing of samples was done in inert gas environment, therefore no oxide layer was formed. The only newly formed layer is the Cr-Zr interlayer. Fig. 2(b) is the cross section morphology of the CS sample after annealing at 1300°C for 60 min, including a residual Cr coating layer, a Cr-Zr interlayer and a Zr substrate layer. All the other CS samples after annealing also show similar cross section structure with different layer thicknesses. The coating structure of the as received MS sample is compact and homogeneous, and the average thickness of the coating is 13.7 $\pm$ 0.1 μm (Fig. 2(c)). Fig. 2(d) is the cross section morphology of the MS sample after annealing at 1300°C for 20 min, which had a similar cross section structure with the CS samples. However, the cross section structure of the MS samples changed with the exposure time increasing. After 60 min annealing at 1300°C (Fig. 2(e)), the Cr coating layer had disappeared and only the Cr-Zr interlayer and the Zr substrate were left. After 120 min annealing at 1300°C,

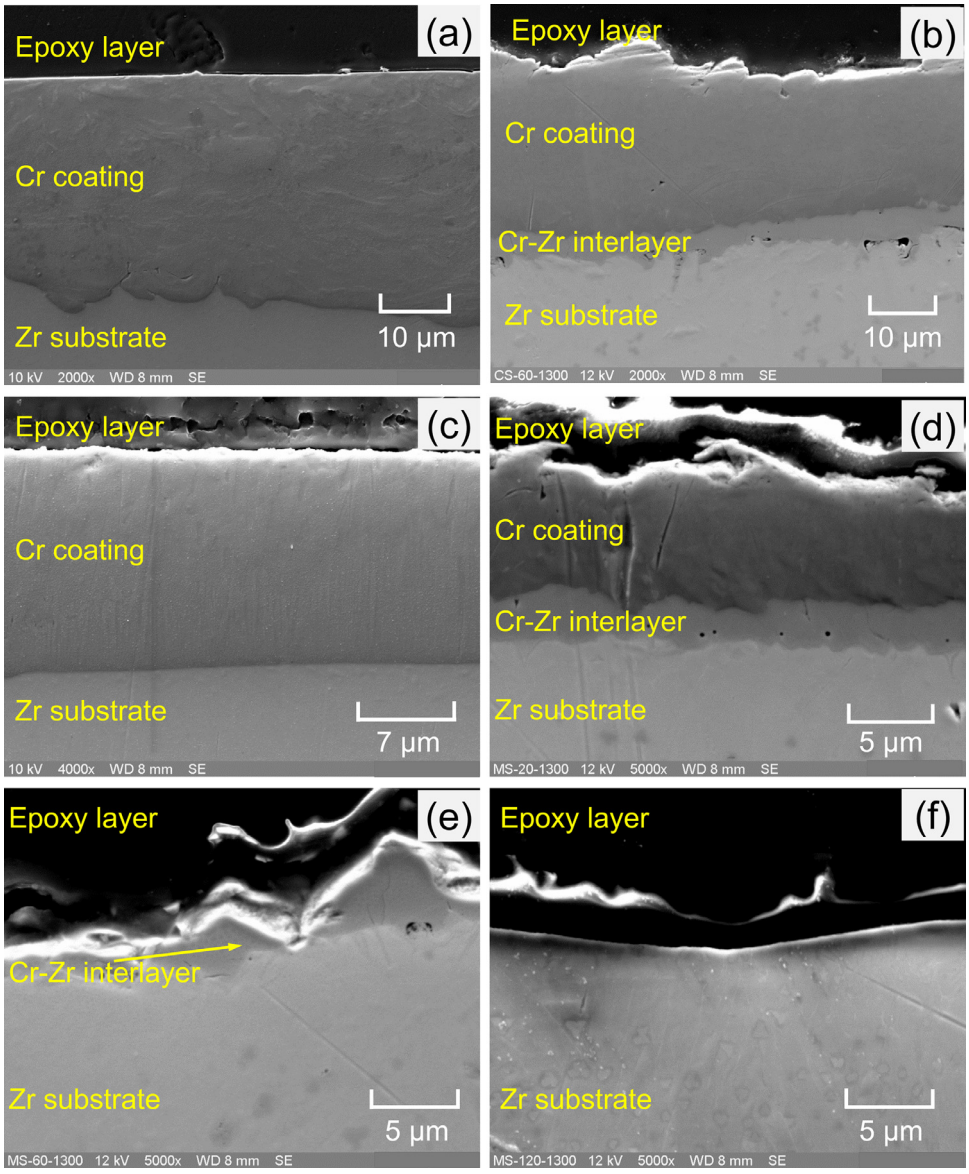

Fig. 2. Cross section morphologies of (a) the as received CS sample, (b) the CS sample after annealing at 1300°C for 60 min, (c) the as received MS sample, (d) the MS samples after annealing at 1300°C for 20 min, (e) the MS samples after annealing at 1300°C for 60 min, and (f) the MS samples after annealing at 1300°C for 120 min. All the CS samples after annealing show similar cross section structures with the CS samples in (b). As for the MS samples, the residual coating layer and Cr-Zr interlayer gradually disappeared due to the limited thickness of the coating.

only the Zr substrate is visible and all the Cr elements were dissolved in the Zr substrate, as shown in Fig. 2(f).

3.2. Growth kinetics of the Cr-Zr interlayer

The samples after annealing at 1100°C, 1200°C and 1300°C were used to study the growth kinetics of Cr-Zr interlayer. Fig. 3 shows the measured thickness of the Cr-Zr interlayer as a function of annealing time and coating method. The thickness of the interlayer is plotted against exposure time, and the error bar represents the standard deviation.

For the samples exposed to 1100°C (Fig. 3(a)), the interlayer grew fast in the first 30 min to about 1 μm, and then the growth rate decreased obviously. An interesting finding for both the CS samples and the MS samples is that the thickness of the Cr-Zr interlayer after 150 min is smaller than that after 120 min. The similar phenomenon was found by Wei et al. [23]. They found that the thickness of the Cr-Zr interlayer in a Cr coated Zry-4 after annealing at 1200°C for 120 min was lower than that after 60 min annealing [23]. This abnormal behavior of the interlayer could be caused by the different diffusion rates of Cr in the Cr-Zr interlayer and the Zr substrate. At high temperatures, the Cr from the coating diffused to the Zr substrate and formed a Cr-Zr interlayer, and then some of the Cr atoms kept diffusing and dissolved in the Zr substrate. Wu et at. [24] and Ribis et at. [25] found that the $Zr(Fe,Cr)_2$ Laves phase was formed in the interlayer. As indicated by Xiang et al. [13] and Nicolai et al. [26], the diffusion coefficient of Cr in the $Zr(Fe,Cr)_2$ phase is five magnitudes smaller than that in the Zr solid solution. Therefore, during the 150 min exposure, the quantity of the Cr atoms diffusing from the Zr-Cr interlayer to the Zr substrate was larger than that from the Cr coating to the interlayer, leading to the diminishing of the thickness of the interlayer.

For the samples annealed at 1200°C (Fig. 3(b)), a similar growth law of the interlayer was observed. The interlayer thickness of the sample at 1200°C is about 0.5 μm to 0.7 μm larger than that at 1100°C after the same exposure time. Similar with the tests at

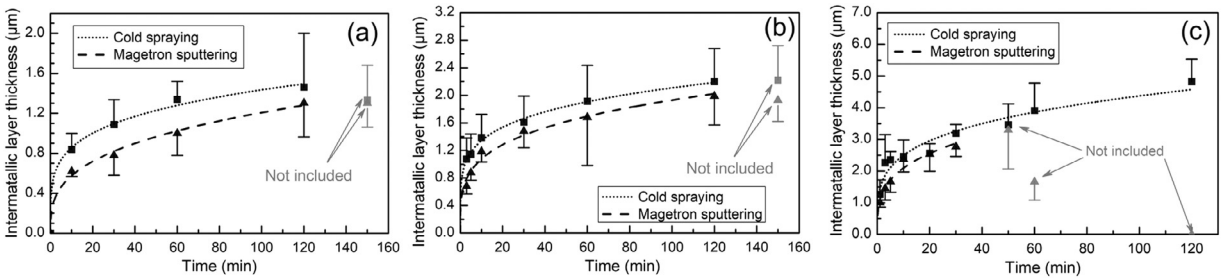

Fig. 3. Measured thickness of the Cr-Zr interlayer as a function of time and coating type at (a) 1100°C, (b) 1200°C and (c) 1300°C.

1100°C, the thickness of the Cr-Zr interlayer in both MS and CS samples after 150 min at 1200°C also decreased compared with that after 120 min exposure.

The growth rate of the Cr-Zr interlayer substantially increased at 1300°C compared those at 1100°C and 1200°C. As shown in Fig. 3, the max value of the Y-scale for the tests, which are 2.0 μm, 3.2 μm and 7.0 μm for the annealing at 1100°C, 1200°C and 1300°C, respectively. The cross section morphology of the MS sample after 60 min exposure at 1300°C (Fig. 2(e)) indicates that the Cr coating disappeared because all the Cr atoms had been consumed by forming the Zr-Cr interlayer and dissolving in the Zr solid solution. When the exposure time increased to 120 min, the interlayer also disappeared because all the Cr from the coating and the interlayer had diffused into the Zr substrate (Fig. 2(f)). The layer evolution process of the MS sample at 1300°C can be considered as an accelerated process of the layer evolution at lower annealing temperatures. Then, the growth behavior of the Cr-Zr interlayer in a Cr coated Zr alloy at high temperature inert gas environment can be summarized as follows:

- Stage 1: The interlayer formed due to the interdiffusion between the coating and the substrate. The thickness of the interlayer kept increasing. Meanwhile, the Cr atoms from the Cr-Zr interlayer began to diffuse and dissolve in the Zr substrate. Due to the difference of diffusion coefficient of Cr in the $Zr(Fe,Cr)_2$ phase and in the Zr solid solution [13,26], the quantity of the Cr atoms diffusing from the Zr-Cr interlayer to the Zr substrate was larger than that from the Cr coating to the interlayer, leading to the diminishing of the thickness of the interlayer. Then, the growth and decomposition of the Cr-Zr interlayer reached a dynamic equilibrium process: the amount of Cr that diffused from Cr coating to the interlayer equals to the amount of Cr that diffused from the interlayer to the Zr substrate, and the thickness of the Cr-Zr interlayer basically remained the same value.
- Stage 2: The Cr coating layer was totally consumed. Then, all the Cr atoms from the Cr coating and the interlayer diffused and dissolved in the Zr substrate. The Cr atoms kept diffusing in the Zr substrate. Finally, the Cr-Zr interlayer gradually disappeared.

Similar with the former studies [9,13], the growth rate of the Cr-Zr interlayer was fitted by a parabolic law at first. However, it seems that the data do not fit to a parabolic law very well. At the beginning of the annealing process, the measured thickness of the Cr-Zr interlayer was higher than the estimated value. The standard heat of formation of $ZrCr_2$, Cr_2O_3 and ZrO_2 is -256 kJ/mol, -1128 kJ/mol, -1080 kJ/mol, respectively [27]. All the diffusion tests were done in inert gas environment, indicating that no Cr_2O_3 or ZrO_2 were formed. Therefore, the difference of the coating thickness between the measured value and the estimated value was not caused by the temperature increasing due to the heat release of the oxidation process, as Yeom et al. [28] explained. The diffusion between

Table 3
Summary of the fitting parameters of the growth of the Cr-Zr interlayer for the MS and CS samples after annealing at 1100°C, 1200°C and 1300°C.

Annealing temperature	Coating method	k / μm × min^{-n}	n
1100°C	MS	0.276	0.321
	CS	0.512	0.224
1200°C	MS	0.598	0.255
	CS	0.852	0.197
1300°C	MS	1.086	0.286
	CS	1.425	0.244

Zr and Cr is a reaction-diffusion process [29]. At the early stage, the growth rate of the interlayer is fast because the growth of interlayer is controlled by chemical reactions between Cr and Zr. The Cr atoms and Zr atoms diffused across its bulk in the opposite direction. Subsequent chemical transformations took place at the interface between the coating and the substrate. As a result, a Cr-Zr interlayer formed [30]. Then, the growth of the interlayer becomes diffusion controlled because the inter-diffusion coefficient gradually decreases with the increasing of the thickness of interlayer. Theoretically, a parabolic law should be observed during that period. However, the parabolic kinetics behavior can be affected by several reasons. For instance, the occurrence of inter-granular back diffusion of Zr in Cr fundamentally differs from simple 1-D volumic thermal diffusion. Moreover, the existence of Kirkendall holes (as already observed at the $ZrCr_2$/Zr interlayer in this study) may modify the actual net diffusion flux of alloy atoms. Therefore, a power law was finally used for the fitting of the growth rate of the Cr-Zr interlayer. Some data that were obviously affected by other processes were eliminated for the fitting, which are shown in gray color in Fig. 3. The relationship of the thickness (δ) of the Cr-Zr interlayer with the annealing time (t) can be written as:

$$\delta = kt^n \tag{1}$$

The values of k and n is summarized in Table 3.

The measured thickness of the Cr-Zr interlayer was lower than the estimated value after a relatively long exposure, such as 120 min. The starting time of this phenomenon changed with different exposure temperature. If the exposure time was long enough, all the residual Cr coating as well as the Cr-Zr interlayer will diffuse and dissolve in the Zr substrate, as what happened with the MS sample after annealing at 1300°C for 120 min. Therefore, although some researchers considered that the growth of the Cr-Zr interlayer obeys a parabolic rule, it should be noted that the parabolic rule is only valid at a specific time interval.

It can be seen that the growth rates of the CS sample are slightly larger than that of the MS sample at the early stage of diffusion, which is related to the existence of oxides on Zr substrate before the coating process. The formation of a very thin oxide layer between a diffusion couple can considerably decrease the growth rate of an interlayer [31,32]. In general, the cold spray process has a ballistic cleaning effect on the initial oxide layer on sub-

Table 4
Summary of the thickness of Cr-Zr interlayer from literatures.

Date source	Coating method	Exposure temperature (°C)	Exposure time (min)	Measured value from literatures (μm)	Measured value from this study (μm)	Estimated value from this study (μm)
Fig. 12(b) from Ref. [2]	Magnetron sputtering	1200	5	0.6	0.9	0.41*
Fig. 6(b) from Ref. [8]	Magnetron sputtering	1200	5	0.6	0.9	0.41*
Fig. 7(a) from Ref. [33]	Magnetron sputtering	1100	30	0.8	0.8	0.72*
Fig. 3(h) from Ref. [34]	Multi arc ion coating	1060	60	0.5	-	0.86*
Fig. 5(a) from Ref. [9]	Cold spray	1310	90	4.6	-	4.79**
Fig. 8(c) from Ref. [23]	Vacuum arc plasma spray	1200	60	4.1	1.9	2.09**
Fig. 5(a) from Ref. [7]	Air plasma spray	1200	60	3	1.9	2.09**

* Estimated from the fitting data of the MS sample
** Estimated from the fitting data of the CS sample

strates due to the very high impact speed of coating particles. For a magnetron sputtering process, the generated coating ions are sputtered on the target in a relatively slower speed under the action of an electric field. Therefore, although no Cr_2O_3 or ZrO_2 thin film were observed at the interface between the Cr coating and the Zr substrate from the as-received MS samples, an original thin oxide layer on the Zr substrate may have survived after the magnetron sputtering process, leading to a relatively slower growth rate of the interlayer.

Some interlayer thickness data from other researches are summarized in Table 4. The thickness of the Cr-Zr interlayer was measured based on the figures given in the literatures. Both the measured thickness and the fitted thickness of the interlayer from this study at the same temperature after the same annealing time are used to compare with the literature date. The results of the comparison are listed as follows:

- Ref. [2] and Ref. [8]: Two different batches of magnetron sputtered samples from CEA were used for these two studies. Although the annealing temperature and time from these two literatures are the same, the thickness of the interlayer is different. Both the two literature values are lower than the measured value from this study. That is to say, the microstructure, which is determined by the operating parameters of the magnetron sputtering process, can also affect the growth rate of the Cr-Zr interlayer.
- Ref. [33]: The literature value is basically the same with the measured value and the fitted value from this study.
- Ref. [34]: Both the multi-arc ion coating method and the magnetron sputtering method belong to physical vapor deposition (PVD) methods, therefore the fitted value from the MS samples is used for comparison. The literature value is lower than the fitted value from this study, indicating that the Cr coating prepared by multi-arc ion coating method has a better diffusion resistance than that prepared by magnetron sputtering method from this study.
- Ref. [9]: The literature value is basically the same with the fitted value from this study.
- Ref. [23] and [7]: Vacuum arc plasma spraying and air plasma spraying belong to plasma spraying method, which is a type of thermal spraying [35]. It can be seen that the interlayer thickness of the samples prepared by thermal spraying is obviously higher than that prepared by cold spraying, maybe due to the easily formed porosity structure in the coating.

3.3. Evaluation of the consumption of the Cr coating

From the former results, it is known that the Cr coating can be consumed by diffusing/dissolving into the Zr substrate besides the interlayer formation. The maximum solubility of Cr in β-Zr is about 8 at.% at 1300°C [36], but the solubility of Cr in α-Zr and of Zr in Cr is less than 2 at.% [37]. In consequence, a considerable amount of Cr atoms diffused through the Cr-Zr interlayer and into the Zr substrate during the high temperature exposure, which also consumed the Cr coating. After each test, the thickness of the residual Cr coating was measured. It can be found that the thickness of the residual Cr coating plus the thickness of the Cr-Zr interlayer does not equal the thickness of the as-received Cr coating. The loss of coating thickness can be roughly considered as the amount of Cr atoms that dissolved in the Zr substrate. According to EDS scanning results (will be discussed in Section 3.4), the Cr-Zr interlayer is composed of $ZrCr_2$. The volume expanded when Cr atoms combined with Zr atoms to form $ZrCr_2$. Therefore, the decrease of coating thickness by forming the interlayer did not equal the increase of the thickness of the interlayer. The thickness of $ZrCr_2$ was converted to original thickness of the Cr layer from structure data by

$$V(ZrCr_2) = R_{ZrCr_2} \times V(Cr) \quad (2)$$

where R_{ZrCr_2} (equals to 1.9) refers to the volume expansion coefficient of Cr atoms to $ZrCr_2$, which was achieved by the same way to calculate the Pilling-Bedworth ratio of metal oxides [38].

Fig. 4 shows the proportion of the residual Cr coating, the interlayer and the dissolution loss for the samples after each exposure. The thickness of the dissolution loss of Cr was obtained by the following equation:

$$V(diffusionloss) = V(originalcoating) - V(residualcoating) - V(Crthatformedthe ZrCr_2) \quad (3)$$

In the Eq. (3), the thickness of the original coating and the residual coating can be directly measured, and the thickness of the Cr layer that formed the $ZrCr_2$ can be calculated by the Eq. (2).

The diffusion loss of Cr in the Zr substrate took a considerable percentage of the coating thickness. Moreover, the portion of the dissolution loss increased with increasing exposure time. The increasing of the dissolution loss seems irregular for the CS samples, especially at the beginning of the exposure. This is due to the uneven interface between the Cr coating layer and the Zr substrate. Fig. 5 shows the cross section of the CS sample after annealing at 1100°C for 10 min. It can be seen that there were some humps at the interface. At the beginning of diffusion, the Cr-Zr interlayer

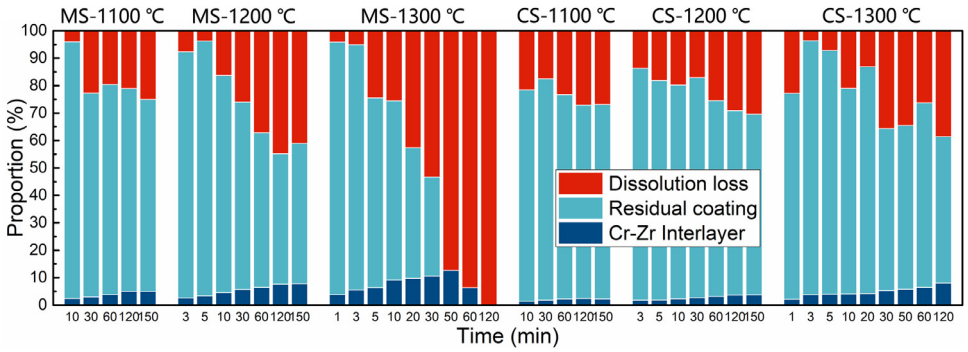

Fig. 4. The proportion of the residual Cr coating, the interlayer and the dissolving loss part of the Cr coating after each exposure.

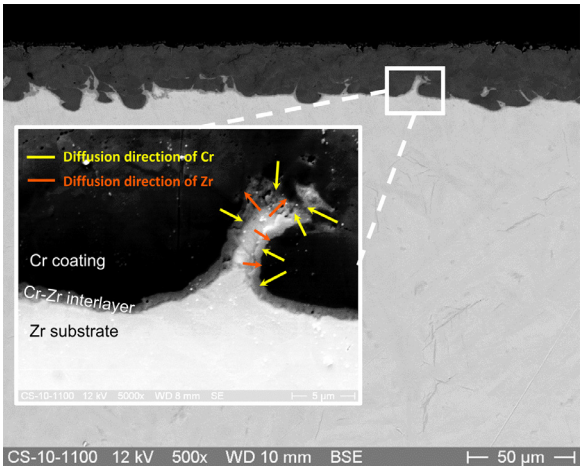

Fig. 5. Cross section morphology of the CS sample after exposure at 1100°C for 10 min. Chromium and zirconium atoms diffused along the direction normal to the interface.

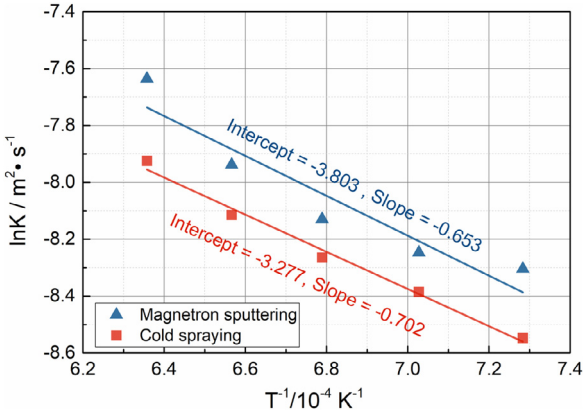

Fig. 6. Arrhenius plot of the consumption coefficient K versus $1/T$ to determine the decreasing rate of Cr coating during annealing at high temperature.

grew along the direction normal to the interface, as shown in the enlarged view in Fig. 5. As a result, the thicknesses of both the residual Cr coating and the Cr-Zr interlayer were fluctuating.

A modified parabolic law valid for diffusion driven processes was used to estimate the consumption of the Cr coating as a combined result of forming a Cr-Zr interlayer and dissolving in the Zr substrate.

The consumption of Cr coating is expressed as

$$X = X_0\sqrt{1 - Kt} \tag{4}$$

where X is the thickness of the residual Cr coating after exposure. X_0 is the thickness of the original Cr coating. For the CS and MS samples, X_0 equals to 31.7 μm and 13.7 μm, respectively. K is defined as the consumption coefficients of the Cr coating, and t is the exposure time in seconds. The equation is valid for $X < X_0$.

By Eq. (4), the consumption coefficients of the Cr coating in different tests were calculated. Ideal situation is that the K for different exposure time at the same exposure temperature is basically the same. However, due to the reaction enhanced diffusion at the beginning, the consumption coefficient was obviously higher than the average value at the first 10 to 20 min. Moreover, the consumption coefficient for the MS sample after 50 min or longer exposure at 1300°C is not valid for such calculation because there is no Cr coating left. Therefore, the consumption coefficient was calculated based on the thickness of the residual Cr coating after 30 min exposure at the temperature range from 1100°C to 1300°C. The temperature dependence of K can be expressed as an Arrhenius type function:

$$K = K_0 \exp\left(-\frac{Q}{RT}\right) \tag{5}$$

where K_0 is the pre-exponential factor and Q is the activation energy. T is the exposure temperature in Kelvin. R=8.314 J/mol·K is the universal gas constant. A plot of ln$K$ versus $1/T$ is shown in Fig. 6, and the data used for fitting is given in Table 5. The values of K_0 and Q were determined by least-squares analysis. Therefore, the consumption of the Cr coating as a combined result of forming a Cr-Zr interlayer and the Eq. (4) describing the dissolution of the coating into the Zr substrate can be extended as:

$$X = X_0\sqrt{1 - K_0 \cdot t \cdot \exp\left(-\frac{Q}{RT}\right)} \tag{6}$$

where K_0 equals to 0.022 and 0.038 m^2/s for the Cr coating prepared by magnetron sputtering and cold spraying, respectively. Q equals to 54.3 and 58.4 kJ/mol for the Cr coating prepared by magnetron sputtering and cold spraying, respectively.

Table 5
The consumption coefficient of the CS and MS coating samples annealing at the temperature range from 1100°C to 1300°C.

T (K)	K (m^2/s)	
	CS sample	MS sample
1373	1.94E-04	2.48E-04
1423	2.28E-04	2.62E-04
1473	2.55E-04	2.95E-04
1523	2.99E-04	3.57E-04
1573	3.62E-04	4.83E-04

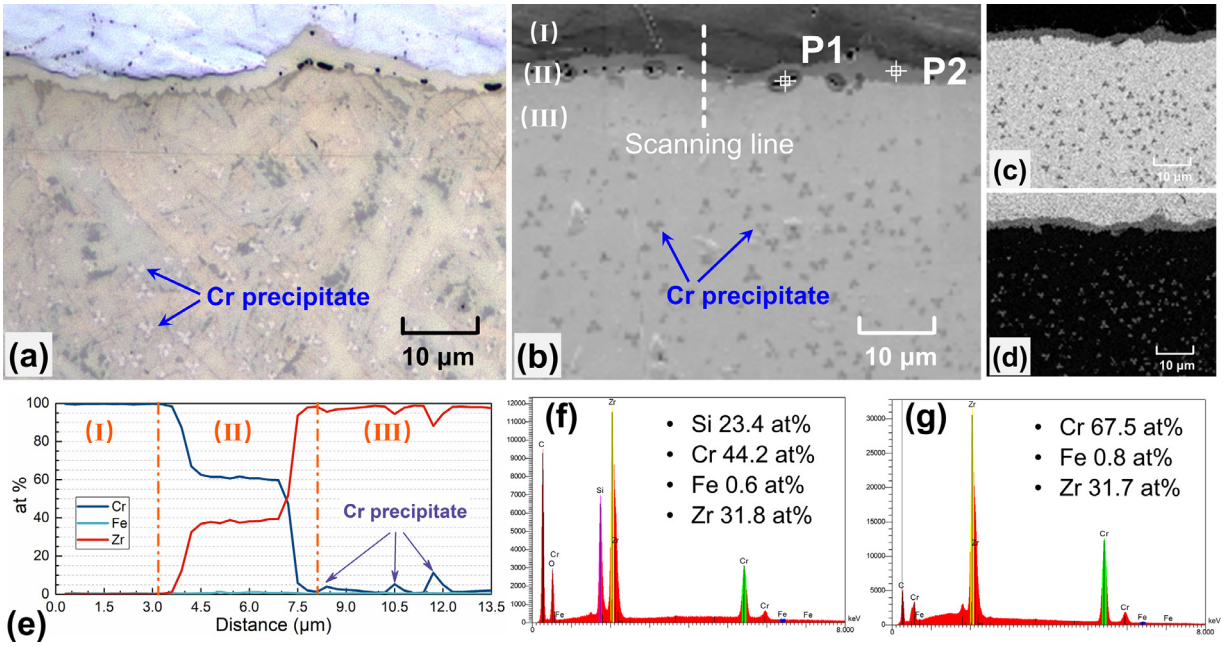

Fig. 7. Cross section morphology and EDS results of the cold spraying Cr coated Zr alloy after 30 min annealing in inert gas at 1300°C. (a) OM image; (b) SEM image; (c) EDS map for Zr; (d) EDS map for Cr; (e) EDS line scanning result; (f) and (g) are the EDS point analyses results of P1 and P2, respectively.

3.4. Morphology and element distribution of the Cr-Zr interlayer

The CS sample after exposure at 1300°C for 30 min is used as an example to show the cross section morphology and the element migration. In Fig. 7(a), the precipitates are mainly inside the lath of Widmanstätten structures, not at the former β-Zr grain boundaries. The dotted precipitation can be seen more distinctively in Fig. 7(b), which is the SEM morphology of the cross section taken at the same location as in Fig. 7(a). The EDS maps of Cr and Zr (Fig. 7(c) and (d)) indicate that the black dots in the Zr substrate are Cr-containing precipitates. The EDS line scanning result (Fig. 7(e)) shows that the Cr-Zr interlayer contains about 60 at% of Cr and about 35 at% of Zr and small amounts of Fe, corresponding to $ZrCr_2$ [24,25].

An interesting finding is that the $ZrCr_2$ precipitations are barely distributed in the Zr substrate near the Cr-Zr interlayer. Although some black dots were observed in the Zr substrate beneath the Cr-Zr interlayer, the size and amount of the Cr precipitations were obviously lower than that in the Zr substrate further away from the Cr-Zr interlayer. This phenomenon can be found on both the MS and the CS samples after annealing. It is supposed that the uneven distribution of the $ZrCr_2$ precipitation was caused by the formation of an α-Zr layer beneath the Cr-Zr interlayer. The oxygen that caused the formation of α-Zr(O) could be the lattice oxygen from the Cr coating, which was trapped in the Cr lattice during the coating growth [39]. Then, the lattice oxygen diffused into the Zr substrate and led to the formation of α-Zr(O). The existence of lattice oxygen was observed in our previous study [40,41] on a MAX phase coating. Moreover, although the heating chamber was kept purging by 6N argon during the high temperature annealing, there may still a small amount of oxygen in the atmosphere. As indicated in the Zr-O phase diagram [42], only about 5 at.% oxygen is needed for the phase transformation from β-Zr to α-Zr at 1300°C. Usually, the α-Zr that is stabilized by oxygen at high temperature is expressed as α-Zr(O). The formation of the α-Zr(O) is often seen in the matrix of Zr alloys after exposure in oxidizing high temperature environment [43,44]. As introduced in Section 3.2, the solubility of Cr in α-Zr is lower than that in β-Zr [45]. During high temperature annealing, the amount of Cr that dissolved in the α-Zr(O) layer was far less than that dissolved in the β-Zr layer. This could be the reason why $ZrCr_2$ precipitations are barely distributed in the Zr substrate near the Cr-Zr interlayer. The low amount of oxygen in the Zr substrate beneath the Cr-Zr interlayer cannot be precisely detected by EDS. Some detection with higher precision, such as wavelength dispersive spectroscopy (WDS), would be done to figure out the oxygen content in the α-Zr(O) layer in the future.

The formation of the holes at the interface of Cr-Zr interlayer and the Zr substrate (Fig. 7(b)) can be explained by the Kirkendall mechanism, and such phenomenon has been reported by several researches on Cr coated ATF cladding [8,46]. As shown in Fig. 7(f), the EDS point scan result for one pore (point "P1" in Fig. 7(b)) indicates that large amounts of Si were concentrated in the hole area. This is due to the polishing process of the samples after the exposure: the samples were grinded by SiC paper and polished by OP-S, which is a colloidal silica suspension with a grain size of about 0.04 μm. Therefore, some Si containing particles were stuck in the pore during the polishing process.

3.5. Distribution of the metallic elements in the bulk alloy

The phase transition of $\alpha \rightarrow \beta$ in a Zry-4 alloy is completed at 910°C [47]. That is to say, the Zr substrate is in the β phase during the high temperature annealing in this study. Extra diffusion tests were done to analyze the precipitation behavior of Cr in Zr substrate. A MS sample was firstly annealed at 1300°C in inert gas environment for 150 min. According to Fig. 4, it can be confirmed that all the Cr coating had been consumed by dissolving in the Zr substrate after 150 min exposure at 1300°C. According to the thickness of the Cr coating and the Zr substrate of the MS sample, it can be roughly calculated that the content of Cr in Zr substrate is about 2.8 wt%, which is less than the saturation solubility of Cr in β-Zr at 1300°C. After exposure, the samples were cooled at two rates:

- Fast cooling: the sample was quickly pulled out from the hot zone in the tube furnace. Then, the furnace was opened and the sample was placed into cold water.

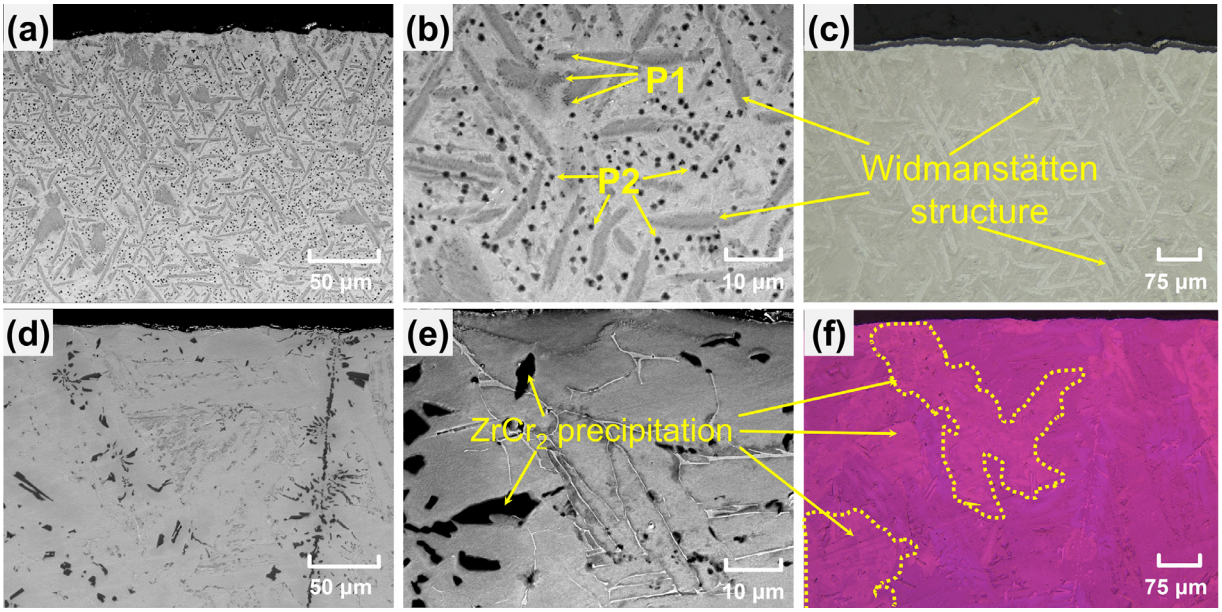

Fig. 8. Microstructure of a MS sample after annealing at 1300°C for 2.5 h and then cooled in (a) fast cooling and (d) slow cooling rate. (b) and (e) is the high magnification figure of (a) and (d), respectively. (c) is a bright-field microscopy of the fast cooling sample, and (f) is a polarized light microscopy of the slow cooling sample.

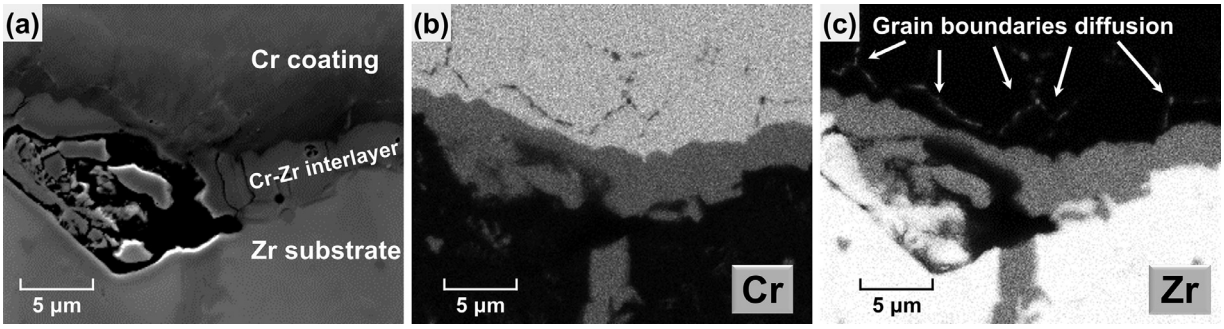

Fig. 9. Cross section morphology of a CS sample after exposure at 1300°C for 30 min. (a) SEM morphology, (b) EDS mapping of Cr, (c) EDS mapping of Zr. A distinct enrichment of Zr along the grain boundaries of Cr is observed.

- Slow cooling: the sample was placed in the furnace after exposure, and the cooling rate of the furnace was set to 3°C/min.

The cross sections of the samples were examined by SEM and OM, as shown in Fig. 8. For the fast cooling sample, non-diffusion phase transition occurred and Widmanstätten structures were formed. Furthermore, α-Zr and $ZrCr_2$ precipitation were formed by the eutectoid decomposition process. There are two sizes of $ZrCr_2$ precipitations, shown as "P1" and "P2" in Fig. 8(b). P1 is located at the front of the phase interface, and P2 is located at the edge of the Widmanstätten structure. Owing to the restricted solubility of Cr in α-Zr, the Widmanstätten structure would be supersaturated [48]. A fraction of Cr atoms would be thrown out from the Zr lattice, forming the precipitation during the fast cooling process [48]. For the slow cooling sample, the α-Zr products generated by β parents are coarse equiaxed grains [49]. As can be seen in the high magnification figure (Fig. 8(e)) and the polarized light microscopy (Fig. 8(f)), a significant extent of precipitation coarsening occurred, forming the large, heterogeneously nucleated and cuboidal precipitates.

Zr atoms can also diffuse into the Cr coating. Fig. 9 shows the cross section morphology of the CS sample after exposure at 1300°C for 30 min. A distinct enrichment of Zr along the grain boundaries of Cr was formed, indicating that the diffusion of Zr in the Cr coating was mainly along the grain boundaries. Moreover, the length of the visible diffusion depth of Zr in the Cr coating is short. This is because the solubility and diffusivity of Zr in Cr are lower than that of Cr in β-Zr [8]. Some Zr atoms may diffuse to a greater distance along the Cr grain boundaries, but a large portion of Zr atoms accumulated at the beginning of the diffusion path (as observed in Fig. 9). The diffusion of Zr along the Cr grain boundaries was also observed by Brachet et al. [8] for a Cr coated Zr alloy after oxidation in high temperature steam environment. In their experiment, inward oxygen diffusion and outward Zr intergranular diffusion occurred in the Cr coating, and ZrO_2 stringers nucleated at the Cr grain boundaries because the thermodynamic stability of ZrO_2 is higher than that of Cr_2O_3.

4. Conclusion

In this study, the Cr-Zr interaction of two types of Cr coated Zr alloy accident tolerant fuel (ATF) cladding, deposited by cold spraying and magnetron sputtering, was studied under inert gas environment in the temperature range from 1100°C to 1300°C. The main conclusions are summarized as follows:

1) A Cr-Zr interlayer formed between the Cr coating layer and the Zr substrate after annealing. A power law was used for the fitting of the growth of the Cr-Zr interlayer. The growth rate of

the interlayer on a cold sprayed sample is slightly larger than that on a magnetron sputtered sample.

2) Except for forming the Cr-Zr interlayer, the Cr coating can be consumed by diffusing/dissolving into the Zr substrate, resulting in the decreasing of the thickness of the interlayer after a relatively long annealing. The dissolution loss of Cr in the Zr substrate takes a considerable percentage of the coating thickness.
3) The consumption coefficients for both types of Cr coating at different temperatures were fitted by Arrhenius equations. Via the equations, the thickness of the residual Cr coating at a given temperature after a given exposure time can be estimated.
4) Cr atoms diffused into the Zr substrate and precipitated as $ZrCr_2$ at the transition of Zr from the β phase to the α phase during the cooling down process. The precipitates are mainly inside the lath of Widmanstätten structures. Moreover, the $ZrCr_2$ precipitations are barely distributed in the Zr substrate near the Cr-Zr interlayer because of the formation of an α-Zr(O) layer between the Cr-Zr interlayer and the Zr substrate. Zr atoms diffused into the Cr coating along grain boundaries. Large portion of the Zr atoms accumulated at the beginning of the diffusion path.

Declaration of Competing Interest

The authors declare that they have no known competing financial interests or personal relationships that could have appeared to influence the work reported in this paper.

CRediT authorship contribution statement

Jianqiao Yang: Investigation, Writing - original draft, Conceptualization, Validation. **Ulrike Stegmaier:** Investigation, Writing - review & editing. **Chongchong Tang:** Conceptualization, Methodology, Writing - review & editing. **Martin Steinbrück:** Conceptualization, Project administration, Writing - review & editing. **Mirco Große:** Conceptualization, Formal analysis, Writing - review & editing. **Shuzhong Wang:** Supervision. **Hans Jürgen Seifert:** Supervision, Writing - review & editing.

Acknowledgments

Jianqiao Yang is supported by China Scholarship Council (No. 201906280319).

The support of this work by the HGF program NUSAFE at Karlsruhe Institute of Technology (KIT) is acknowledged.

The authors thank Petra Severloh for her support in the sample preparation and optical metallography investigations.

References

[1] C. Tang, M. Stueber, H.J. Seifert, M. Steinbrück, Protective coatings on zirconium-based alloys as accident-tolerant fuel (ATF) claddings, 35 (2017) 141.
[2] J.-C. Brachet, I. Idarraga-Trujillo, M.Le Flem, M.Le Saux, V. Vandenberghe, S. Urvoy, E. Rouesne, T. Guilbert, C. Toffolon-Masclet, M. Tupin, C. Phalippou, F. Lomello, F. Schuster, A. Billard, G. Velisa, C. Ducros, F. Sanchette, Early studies on Cr-Coated Zircaloy-4 as enhanced accident tolerant nuclear fuel claddings for light water reactors, J. Nucl. Mater. 517 (2019) 268–285.
[3] J. KREJČÍ, M. ŠEVEČEK, J. Kabatova, F. Manoch, J. KOČÍ, L. CVRČEK, J. Malek, S. Krum, P. ŠUTTA, P. Bublikova, Experimental behavior of chromium-based coatings, Proc. TopFuel (2018).
[4] J. Bischoff, C. Vauglin, C. Delafoy, P. Barberis, D. Perche, B. Guerin, J.P. Vassault, J.C. Brachet, Development of Cr-coated zirconium alloy cladding for enhanced accident tolerance, Topfuel 2016-Light Water Reactor (LWR) Fuel Performance Meeting, 2016.
[5] H.-G. Kim, I.-H. Kim, Y.-I. Jung, D.-J. Park, J.-Y. Park, Y.-H. Koo, in: High-Temperature Oxidation Behavior of Cr-Coated Zirconium Alloy, In: Proceeding of LWR Fuel Performance Meeting/Topfuel, Charlotte, USA, 2013, pp. 842–846.
[6] J.-H. Park, H.-G. Kim, J.-y. Park, Y.-I. Jung, D.-J. Park, Y.-H. Koo, High temperature steam-oxidation behavior of arc ion plated Cr coatings for accident tolerant fuel claddings, Surf. Coat. Technol. 280 (2015) 256–259.
[7] Y. Wang, W. Zhou, Q. Wen, X. Ruan, F. Luo, G. Bai, Y. Qing, D. Zhu, Z. Huang, Y. Zhang, T. Liu, R. Li, Behavior of plasma sprayed Cr coatings and FeCrAl coatings on Zr fuel cladding under loss-of-coolant accident conditions, Surf. Coat. Technol. 344 (2018) 141–148.
[8] J.-C. Brachet, E. Rouesne, J. Ribis, T. Guilbert, S. Urvoy, G. Nony, C. Toffolon-Masclet, M.Le Saux, N. Chaabane, H. Palancher, A. David, J. Bischoff, J. Augereau, E. Pouillier, High temperature steam oxidation of chromium–coated zirconium-based alloys: Kinetics and process, Corros. Sci. 167 (2020) 108537.
[9] H. Yeom, B. Maier, G. Johnson, T. Dabney, M. Lenling, K. Sridharan, High temperature oxidation and microstructural evolution of cold spray chromium coatings on Zircaloy-4 in steam environments, J. Nucl. Mater. 526 (2019) 151737.
[10] E.B. Kashkarov, D.V. Sidelev, M.S. Syrtanov, C. Tang, M. Steinbrück, Oxidation kinetics of Cr-coated zirconium alloy: Effect of coating thickness and microstructure, Corros. Sci. 175 (2020) 108883.
[11] J. Krejčí, J. Kabátová, F. Manoch, J. Kočí, L. Cvrček, J. Málek, S. Krum, P. Šutta, P. Bublíková, P. Halodová, H.K. Namburi, M. Ševeček, Development and testing of multicomponent fuel cladding with enhanced accidental performance, Nucl. Eng. Technol. 52 (2020) 597–609.
[12] J.-C. Brachet, M.Le Saux, V. Lezaud-Chaillioux, M. Dumerval, Q. Houmaire, F. Lomello, F. Schuster, E. Monsifrot, J. Bischoff, E. Pouillier, Behavior under LOCA conditions of enhanced accident tolerant chromium coated zircaloy-4 claddings, Topfuel 2016-Light Water Reactor (LWR) Fuel Performance Meeting, 2016.
[13] W. Xiang, S. Ying, Reaction diffusion in chromium-zircaloy-2 system, China Nuclear Information Centre, CNIC–01562, (2001).
[14] K. Pettersson, H. Chung, M. Billone, T. Fuketa, F. Nagase, C. Grandjean, G. Hache, J. Papin, L. Heins, Z. Hozer, Nuclear Fuel Behaviour in Loss-of-coolant Accident (LOCA) Conditions, in, Organisation for Economic Co-Operation and Development, 2009.
[15] K.A. Terrani, Accident tolerant fuel cladding development: promise, status, and challenges, J. Nucl. Mater. 501 (2018) 13–30.
[16] H. Yeom, T. Dabney, G. Johnson, B. Maier, M. Lenling, K. Sridharan, Improving deposition efficiency in cold spraying chromium coatings by powder annealing, Int. J. Adv. Manuf. Technol. 100 (2019) 1373–1382.
[17] B. Maier, H. Yeom, G. Johnson, T. Dabney, J. Walters, P. Xu, J. Romero, H. Shah, K. Sridharan, Development of cold spray chromium coatings for improved accident tolerant zirconium-alloy cladding, J. Nucl. Mater. 519 (2019) 247–254.
[18] D.V. Sidelev, G.A. Bleykher, M. Bestetti, V.P. Krivobokov, A. Vicenzo, S. Franz, M.F. Brunella, A comparative study on the properties of chromium coatings deposited by magnetron sputtering with hot and cooled target, Vacuum 143 (2017) 479–485.
[19] D.V. Sidelev, G.A. Bleykher, V.P. Krivobokov, Z. Koishybayeva, High-rate magnetron sputtering with hot target, Surf. Coat. Technol. 308 (2016) 168–173.
[20] M. Ševeček, A. Gurgen, A. Seshadri, Y. Che, M. Wagih, B. Phillips, V. Champagne, K. Shirvan, Development of Cr cold spray–coated fuel cladding with enhanced accident tolerance, Nucl. Eng. Technol. 50 (2018) 229–236.
[21] M. Steinbrück, Oxidation of boron carbide at high temperatures, J. Nucl. Mater. 336 (2005) 185–193.
[22] JEOL, Smileview software, in.
[23] T. Wei, R. Zhang, H. Yang, H. Liu, S. Qiu, Y. Wang, P. Du, K. He, X. Hu, C. Dong, Microstructure, corrosion resistance and oxidation behavior of Cr-coatings on Zircaloy-4 prepared by vacuum arc plasma deposition, Corros. Sci. 158 (2019) 108077.
[24] A. Wu, J. Ribis, J.C. Brachet, E. Clouet, F. Leprêtre, E. Bordas, B. Arnal, HRTEM and chemical study of an ion-irradiated chromium/zircaloy-4 interface, J. Nucl. Mater. 504 (2018) 289–299.
[25] J. Ribis, A. Wu, J.C. Brachet, F. Barcelo, B. Arnal, Atomic-scale interface structure of a Cr-coated Zircaloy-4 material, J. Mater. Sci. 53 (2018) 9879–9895.
[26] L. Nicolai, R. de Tendler, Chromium diffusion in zircaloy-4, J. Nucl. Mater. 82 (1979) 439–443.
[27] Q. Yao, H. Xing, S. Liu, J. Sun, Theoretical prediction of ternary site occupancies in ZrCr2 and NbCr2 laves phases, Mater. Sci. Forum, Trans. Tech. Publ. (2007) 1451–1454.
[28] H. Yeom, B. Maier, G. Johnson, T. Dabney, M. Lenling, K. Sridharan, High temperature oxidation and microstructural evolution of cold spray chromium coatings on Zircaloy-4 in steam environments, J. Nucl. Mater. 526 (2019) 11.
[29] M. Kajihara, Analysis of kinetics of reactive diffusion in a hypothetical binary system, Acta Mater 52 (2004) 1193–1200.
[30] V.I. Dybkov, Reaction Diffusion and Solid State Chemical Kinetics, Trans Tech Publ, 2002.
[31] K. Bhanumurthy, W. Krauss, J. Konys, Solid-state diffusion reaction and formation of intermetallic phases in the Fe-Al system, Fusion Sci. Technol. 65 (2014) 262–272.
[32] V. Jindal, V.C. Srivastava, A. Das, R.N. Ghosh, Reactive diffusion in the roll bonded iron–aluminum system, Mater. Lett. 60 (2006) 1758–1761.
[33] J. Krejčí, M. Ševeček, L. Cvrcek, J. Kabátová, F. Manoch, Chromium and chromium nitride coated cladding for nuclear reactor fuel, in: Proceedings of the 20th International Corrosion Congress, 2017, p. 2017. EUROCORR.
[34] X. He, Z. Tian, B. Shi, X. Xu, C. Meng, W. Dang, J. Tan, X. Ma, Effect of gas pressure and bias potential on oxidation resistance of Cr coatings, Ann. Nucl. Energy 132 (2019) 243–248.
[35] P. Fauchais, Understanding plasma spraying, J. Phys. D 37 (2004) R86.
[36] K. Zeng, M. Hamalainen, R. Luoma, A thermodynamic assessment of the Cr–Zr system, Zeitschrift fur Metallkunde(Germany) 84 (1993) 23–28.

[37] N. Dupin, I. Ansara, C. Servant, C. Toffolon, C. Lemaignan, J.C. Brachet, A thermodynamic database for zirconium alloys, J. Nucl. Mater. 275 (1999) 287–295.
[38] D.J. Young, High Temperature Oxidation and Corrosion of Metals, Elsevier, 2008.
[39] O. Wilhelmsson, J.P. Palmquist, E. Lewin, J. Emmerlich, P. Eklund, P.O.Å. Persson, H. Högberg, S. Li, R. Ahuja, O. Eriksson, L. Hultman, U. Jansson, Deposition and characterization of ternary thin films within the Ti–Al–C system by DC magnetron sputtering, J. Cryst. Growth 291 (2006) 290–300.
[40] C. Tang, M. Klimenkov, U. Jaentsch, H. Leiste, M. Rinke, S. Ulrich, M. Steinbrück, H.J. Seifert, M. Stueber, Synthesis and characterization of Ti2AlC coatings by magnetron sputtering from three elemental targets and ex-situ annealing, Surf. Coat. Technol. 309 (2017) 445–455.
[41] C. Tang, M. Steinbrück, M. Klimenkov, U. Jäntsch, H.J. Seifert, S. Ulrich, M. Stüber, Textured growth of polycrystalline MAX phase carbide coatings via thermal annealing of M/C/Al multilayers, J. Vacuum Sci. Technol. A 38 (2020) 013401.
[42] R. Arroyave, L. Kaufman, T.W. Eagar, Thermodynamic modeling of the Zr-O system, Calphad 26 (2002) 95–118.
[43] M. Steinbrück, J. Birchley, A.V. Boldyrev, A.V. Goryachev, M. Grosse, T.J. Haste, Z. Hózer, A.E. Kisselev, V.I. Nalivaev, V.P. Semishkin, L. Sepold, J. Stuckert, N. Vér, M.S. Veshchunov, High-temperature oxidation and quench behaviour of Zircaloy-4 and E110 cladding alloys, Prog. Nucl. Energy 52 (2010) 19–36.
[44] A. Michau, F. Maury, F. Schuster, F. Lomello, J.C. Brachet, E. Rouesne, M.Le Saux, R. Boichot, M. Pons, High-temperature oxidation resistance of chromium-based coatings deposited by DLI-MOCVD for enhanced protection of the inner surface of long tubes, Surf. Coat. Technol. 349 (2018) 1048–1057.
[45] D. Arias, J. Abriata, The Cr−Zr (Chromium-Zirconium) system, bulletin of alloy phase diagrams, 7 (1986) 237-244.
[46] X. Han, J. Xue, S. Peng, H. Zhang, An interesting oxidation phenomenon of Cr coatings on Zry-4 substrates in high temperature steam environment, Corros. Sci. 156 (2019) 117–124.
[47] J. Ni, Y. Zhao, L. Wang, Z. Zhang, J. Xie, Microstructure of Zircaloy-4 alloy during β phase quenching and determination of critical quenching diameter of its rods, Nucl. Mater. Energy 17 (2018) 158–163.
[48] P. Mukhopadhyay, V. Raman, S. Banerjee, R. Krishnan, Tempering of a beta quenched Zr-1.9 wt % Cr alloy, J. Mater. Sci. 14 (1979) 1389–1397.
[49] Y.H. Jeong, K.S. Rheem, C.S. Choi, Y.S. Kim, Effect of Beta Heat Treatment on Microstructure and Nodular Corrosion of Zircaloy-4, J. Nucl. Sci. Technol. 30 (1993) 154–163.